THE JOURNAL OF BIOLOGICAL CHEMISTRY VOL. 285, NO. 13, pp. 10030–10043, March 26, 2010
Printed in the U.S.A.

Pro-hormone Secretogranin II Regulates Dense Core Secretory Granule Biogenesis in Catecholaminergic Cells*[S]

Received for publication, September 9, 2009, and in revise form, December 16, 2009 Published, JBC Papers in Press, January 8, 2010, DOI 10.1074/jbc.M109.064196

Maïté Courel[‡1], Alex Soler-Jover[‡], Juan L. Rodriguez-Flores[‡], Sushil K. Mahata[‡§], Salah Elias[¶], Maïté Montero-Hadjadje[¶], Youssef Anouar[¶], Richard J. Giuly[‖], Daniel T. O'Connor[‡§2], and Laurent Taupenot[‡§3]

From the [‡]Department of Medicine, University of California San Diego, La Jolla, California 92093-0838, [¶]INSERM U982, University of Rouen, 76821 Mont-St.-Aignan Cedex, France, [‖]National Center for Microscopy and Imaging Research, University of California San Diego, La Jolla, California 92093, and [§]Veteran Affairs San Diego Healthcare System, San Diego, California 92093

Processes underlying the formation of dense core secretory granules (DCGs) of neuroendocrine cells are poorly understood. Here, we present evidence that DCG biogenesis is dependent on the secretory protein secretogranin (Sg) II, a member of the granin family of pro-hormone cargo of DCGs in neuroendocrine cells. Depletion of SgII expression in PC12 cells leads to a decrease in both the number and size of DCGs and impairs DCG trafficking of other regulated hormones. Expression of SgII fusion proteins in a secretory-deficient PC12 variant rescues a regulated secretory pathway. SgII-containing dense core vesicles share morphological and physical properties with *bona fide* DCGs, are competent for regulated exocytosis, and maintain an acidic luminal pH through the V-type H^+-translocating ATPase. The granulogenic activity of SgII requires a pH gradient along this secretory pathway. We conclude that SgII is a critical factor for the regulation of DCG biogenesis in neuroendocrine cells, mediating the formation of functional DCGs via its pH-dependent aggregation at the *trans*-Golgi network.

Derangements of catecholamine storage and release have been widely implicated in human cardiovascular disease risk (1, 2). Catecholamines are stored, together with peptides hormones and neuropeptides, within large dense core secretory granules (DCGs)[4] in chromaffin cells and noradrenergic nerves, until prompted to undergo exocytotic release in response to stimulation (3). The molecular mechanisms and regulatory processes controlling the biogenesis of DCGs, and therefore catecholamine storage and release, remain poorly understood.

The major soluble components of DCGs are the granin protein family of secreted pro-hormones (4), including chromogranin A (CgA), chromogranin B (CgB), and secretogranin (Sg) II. Because of their abundance and their capacity to aggregate *in vitro* with matrix proteins and to interact with the vesicle membrane in environmental conditions found in the *trans*-Golgi network (TGN) (*e.g.* presence of millimolar Ca^{2+} and pH 5.5 (5–8)), granins have long been proposed to contribute to some aspect of the formation of DCGs (9). *In vitro* and *in vivo* evidence now suggests that CgA plays a critical role in the process. Depletion of CgA in PC12 cells reduces the number of DCGs (10–12) and the intracellular levels of other granule proteins (12, 13). Impaired expression of CgA in transgenic mice decreases the number of DCGs in the adrenal medulla and perturbs the storage and release of other DCG constituents, including CgB, neuropeptide Y (NPY), and catecholamines (13, 14). Yet another CgA null mouse strain shows no phenotype changes of DCGs in the adrenal medulla (15). However, the observed substantial increase of CgB and SgII expression in knock-out animals suggests that CgB and/or SgII might partly compensate for CgA deficiency (15). Indeed, CgB depletion in PC12 cells may contribute to an 80% decreased number of DCGs (11), although CgB seems unable to rescue a regulated secretory pathway in secretory-deficient neuroendocrine cells (12, 16). A granulogenic role for CgA and CgB is also documented across cell lineages, where their expression induces the formation of granule-like structures competent for exocytosis (11, 12, 17–20).

The granin SgII is prominent within both human and rodent secretory granules, including catecholamine storage vesicles (21), but little is known about its granule forming activity in neuroendocrine cells. Evidence gathered so far reports the formation of granule-like structures in the fibroblast-like COS-1 cell line (19), and a vesicular distribution of secretoneurin immunoreactivity in ischemic mouse muscle fibers (22). Common genetic variation at the human *SCG2* locus modulates SgII

* This work was supported, in whole or in part, by National Institutes of Health Grants HL58120, DK60702, and DK59628. This work was also supported by postdoctoral research fellowships from the Fondation pour la Recherche Médicale and the National Kidney Foundation (to M. C.), the Comissionat per Universitat I Recerca of the Departament d'Innovació, Universitats i Empresa of the Autonomous Government of Catalonia (to A. S.-J.), and by American Heart Association Grant 0855181F.

[S] The on-line version of this article (available at http://www.jbc.org) contains supplemental Figs. S1 and S2.

[1] To whom correspondence may be addressed: INSERM U982, University of Rouen, 76821 Mont-Saint-Aignan Cedex, France. Fax: 33-2-3514-6946; E-mail: mcourel@univ-rouen.fr.

[2] To whom correspondence may be addressed: University of California at San Diego, School of Medicine, Dept. of Medicine (0838), La Jolla, CA 92093-0838. Fax: 858-534-0626; E-mail: doconnor@ucsd.edu.

[3] To whom correspondence may be addressed: National Institutes of Health, 6701 Rockledge Dr., Bethesda, MD 20892-7850. E-mail: ltaupenot@gmail.com.

[4] The abbreviations used are: DCG, dense core secretory granule; TGN, *trans*-Golgi network; CgA, chromogranin A; CgB, chromogranin B; Sg, secretogranin; NPY, neuropeptide Y; L-BoNT/C1, botulinum neurotoxin C1 light chain; V-ATPase, V-type H^+-translocating ATPase; SIG, SgII signal peptide; EAP, embryonic alkaline phosphatase; RFP, monomeric red fluorescent protein; TIRFM, total internal reflection fluorescence microscopy; MSD, mean square displacement; BafA1, bafilomycin A1; Ct, control (siRNA); DMEM, Dulbecco's modified Eagle's medium; FBS, fetal bovine serum; HA, hemagglutinin; MES, 4-morpholineethanesulfonic acid; siRNA, small interfering RNA; GFP, green fluorescent protein; BAPTA/AM, 1,2-bis-(*o*-aminophenoxy)-ethane-*N*,*N*,*N*′,*N*′-tetraacetic acid, tetraacetoxymethyl ester.

transcriptional expression, which correlates with blood pressure elevation (2). Why are such quantitative alterations important for systemic hypertension? If, like CgA, SgII plays a role in the formation of catecholamine storage vesicles, then a mechanistic link between SgII variation and cardiovascular disease would become plausible. Here, we provide a molecular definition of the DCG-forming function of SgII in neuroendocrine cells by probing whether additive or subtractive changes in SgII expression have consequences for DCG formation.

EXPERIMENTAL PROCEDURES

Construction of Expression Vectors—Expression plasmids for GFP or a truncated form of embryonic alkaline phosphatase (EAP) fused to the carboxyl terminus of full-length human SgII (NM_003469), including its predicted 30-residue signal peptide SIG (SgII-GFP and SgII-EAP), or to SgII signal peptide alone (SIG-GFP and SIG-EAP) were described previously (23). A cDNA encoding a monomeric form of RFP gene (gift from Roger Tsien (24)) was amplified with specific primers incorporating a KpnI restriction site at the 3′ end and a NotI restriction site at the 5′ end. The fragment was subcloned in-frame into the same sites of pCMV-SgII-GFP to produce pCMV-SgII-RFP. pCMV-SgII-EGFP served as a template to amplify full-length SgII flanked by XhoI and KpnI restriction sites at the 5′ and 3′ ends, respectively. The amplified SgII fragment was subcloned into the same sites of pCMV-CgA-HA (10) to produce pCMV-SgII-HA. pCMV-SgII-HA was digested with NheI and NotI, and the resulting fragment was cloned into the same sites of pcDNA3.1/Hygro(+) (Invitrogen) to produce pcDNA-SgII-HA. All plasmids were verified by restriction and DNA sequencing. A vector encoding NPY fused to GFP was a gift from Richard Mains (pre-NPY-GFP (25)). A plasmid encoding botulinum C1 light chain (pCDN3-BoNT/C1) was a gift from Robert Burgoyne (26). Plasmids pECFP-Golgi and pECFP-C1 were purchased from Clontech.

Cell Culture—Pheochromocytoma PC12 cells, the variant sympathoadrenal cell line A35C (27), and the African green monkey kidney fibroblast-derived COS-7 cells (ATCC, CRL 1651) were routinely grown as described previously (10, 20). Most experiments were performed on cells plated onto either poly-L-lysine (Sigma) plus collagen (Upstate)-coated 15-mm round glass coverslips (Fischer No. 1) in 12-well Costar plates or onto poly-L-lysine-coated 6- or 12-well plates.

The A35C-S7 clonal cell line that stably expresses SgII-HA was obtained upon transfection of A35C cells with pcDNA-SgII-HA followed by a selection with hygromycin B (800 μg/ml, Invitrogen). Hygromycin B-resistant clones were screened for SgII-HA expression by immunoblotting and immunofluorescence microscopy. The A35C-S7 clone showed ~80% of cells expressing SgII-HA and was maintained in 500 μg/ml hygromycin B-containing medium until further experiments. The corresponding control cell line, transfected with the pcDNA3.1/Hygro(+) vector, was obtained and cultured in the same conditions.

Transfection and siRNA Gene Silencing—PC12 or A35C cells were transfected with supercoiled plasmid DNA using GenePorter 2 (gelatins) as described previously (28). COS-7 cells were transfected using Lipofectamine 2000 (Invitrogen) according to the manufacturer's protocol. SgII siRNA duplex was designed with the siDESIGN algorithm (Dharmacon), based on an AA(N19)TT pattern. The siDESIGN algorithm (29) uses eight criteria to facilitate knockdown while minimizing off-target oligonucleotide effects. Sequences of the siRNA oligonucleotides for rat SgII based on the reference mRNA sequence accession number NM_022669 were as follows: 5′-GAAGUUUCCUAGUCCAGAAdTdT-3′ and antisense 5′-UUCUGGACUAGGAAACUUCdTdT-3′. BLAST of the rat genome indicated that these oligonucleotide sequences were unique to the intended SgII target. Previous studies have demonstrated that even a single base mismatch is sufficient to abrogate the effect of an siRNA (30). Oligonucleotides were synthesized and annealed by Sigma-Proligo. To further guard against off-target oligonucleotide effects, the Silencer Negative Control 1 siRNA (siRNA-Ct, Ambion), designed to have no significant sequence similarity to mouse, rat, or human transcript sequences, was used as negative control in the transfections. PC12 cells were transfected with 4 μg (12-well plate) of siRNA-SgII or siRNA-Ct, using RNAiFect transfection reagent (Qiagen) at a 1:6 ratio. The culture medium was replaced 5–8 h after the beginning of the transfection, and cells were further cultured for 96 h.

Fluorescence Imaging and Immunocytochemistry—Transfected PC12 and A35C cells were processed for deconvolution fluorescence microscopy and immunocytochemistry as described previously (23). Mitochondrial staining was achieved using MitoTracker red CMXRos (Molecular Probes). For immunocytochemistry, the primary antibodies were a rabbit polyclonal anti-human placental alkaline phosphatase antibody (1:50; Biomeda), a rabbit polyclonal anti-human SgII (1:250 (31)), a rabbit polyclonal anti-LGP110 (1:1000 (32)), a rabbit polyclonal anti-EEA1 (1:100; BD Transduction Laboratories), or a mouse monoclonal anti-HA antibody (1:1000; Covance). Secondary antibodies were an Alexa Fluor 594-conjugated goat anti-rabbit IgG $(F(ab')_2$ at 1:250; Molecular Probes) or a fluorescein-conjugated goat anti-mouse IgG $(F(ab')_2$ at 1:350; Biodesign International).

Images were captured on a DeltaVision deconvolution microscopy system (Applied Precision) as described previously (23). Briefly, optical *xy* sections along the *z* axis were acquired with increments of 0.2 μm and deconvolved to generate optical sections and three-dimensional images of the data sets. The following excitation and emission wavelengths were used for imaging: GFP and fluorescein-conjugated antibodies (green), λ_{ex} 490 ± 10/λ_{em} 528 ± 38 nm; RFP, MitoTracker, and Alexa Fluor 594 antibodies (red), λ_{ex} 555 nm/λ_{em} 580 nm; CFP (blue), λ_{ex} 436 ± 10/λ_{em} 465 ± 30 nm; Hoechst 33342 (nuclear DNA stain, blue), λ_{ex} 350/λ_{em} 461 nm. COS-7 cells were observed on a Leica SP2 upright confocal laser scanning microscope (DMRAX-UV) equipped with the Acousto-Optical Beam Splitter system and with 25, 40, and 63× oil immersion objectives (Leica, Microsystems, Reuil-Malmaison, France) as described previously (20).

Quantification of Fluorescence Co-localization—The extent of co-localization between fluorescence signals was analyzed as described previously (23) using the pixel-per-pixel localization algorithm of ImageMaster software (Photon Technology Inter-

national), which uses Image-Pro as a backbone (Media Cybernetics). The averaged Pearson correlation coefficient (R_p) and overlap coefficient (R_o) of each cell, quantitative of the degree of overlap between two S1 and S2 fluorescent signals, were used for statistical analysis of variance by Dunnett's post test.

Electron Microscopy—Cells were processed for morphological electron microscopy as described previously (10). For immunogold labeling of SgII-HA in A35C-S7 cells, samples were processed for ultrathin cryosectioning as described (33). SgII-HA was detected using a mouse monoclonal anti-HA antibody (1:50; Covance) followed by a 10 nm gold-conjugated goat anti-mouse secondary antibody (1:25; EY Laboratories). Images were acquired with a JEOL 1200 EX II electron microscope, and post-imaging analysis was performed using ImageJ. DCGs in PC12 cells and electron-dense vesicular structures positive for SgII-HA in A35C-S7 cells were circled and counted. The diameter of each vesicle was calculated as the mean of the diameter inferred from the perimeter and the diameter inferred from the area of each drawn circle. 15 micrographs from PC12 cells and 34 micrographs of SgII-positive vesicular structures in A35C-S7 cells were used for the analyses. The area of PC12 cytoplasm was calculated by measuring the area of the entire cell minus the area occupied by the nucleus, and the density of DCGs was calculated by dividing the number of granules by the area of cytoplasm.

Measurement of Intravesicular pH—PC12 or A35C cells grown on poly-L-lysine- and collagen-coated 25-mm round glass coverslips (Warner Instruments) were transfected with pCMV-SgII-EGFP and transferred into a perfusion chamber (Quick Exchange, Warner Instruments). Monitoring of single cell fluorescence was achieved with ImageMaster IM-2103-6-HQ imaging system (Photon Technology International), including a Nikon TS100 inverted microscope, a DeltaRAM monochromator, and a CoolSnap HQ CCCD camera (Photometrics). Filters used were a 505DRLP dichroic XF2010 and a 535AF45 emitter XF3084 (Omega Optical). Cells were incubated in calcium saline buffer (CaB: 140 mM NaCl, 5.4 mM KCl, 0.8 mM $MgCl_2$, 5 mM $CaCl_2$, 10 mM glucose, 10 mM HEPES, pH 7.4) in which bafilomycin A1 (BafA1, LLC Laboratories) was added to a 100 nM final concentration. At the end of each experiment, algebraic conversion of GFP fluorescence to pH value was obtained *in situ* by incubating the cells for 3 min in KCl-rich media (125 mM KCl, 20 mM NaCl, 0.5 mM $CaCl_2$, 0.5 mM $MgCl_2$, 5 μM monensin, 5 μM nigericin, 25 mM of MES or Tris) buffered to pH values ranging from 4.5 to 8 (at a 0.5 pH unit interval). For some KCl depolarization experiments, cells were incubated in a buffer devoid of Ca^{2+} (−CaB: 140 mM NaCl, 5.4 mM KCl, 0.8 mM $MgCl_2$, 10 mM glucose, 10 mM HEPES, pH 7.4), and the following reagents were superfused into the CaB or −CaB buffers: 50 mM KCl, 50 mM 1,2-bis-(*o*-aminophenoxy)-ethane-*N,N,N′,N′*-tetraacetic acid, tetraacetoxymethyl ester, cell permeant derivative (BAPTA/AM, Calbiochem).

Total Internal Reflection Fluorescence Microscopy (TIRFM)—Cells expressing SgII-GFP were grown onto poly-L-lysine- and collagen-coated 35-mm glass bottom culture dishes (MatTek) and washed with serum-free DMEM prior to imaging performed at room temperature on a custom system, including an inverted Nikon TE300 fitted with a ×60 high numerical aperture objective lens (Nikon Plan Apo, N.A 1.45). Excitation was produced by an argon/krypton ion laser (Melles Griott Multiline), and incident light for total internal reflection illumination was introduced from the high numerical aperture objective lenses. Images were acquired on an EMCCD Cascade II camera (Photometrics) controlled by Image-Pro Plus 5.0 software (Media Cybernetics). The value of the penetration depth of the evanescent wave used to excite GFP was estimated to be ~140 nm in the *z* axis after calibration using 2-μm fluorescent polymer microspheres. Exposure times were 100–200 ms, and frames were acquired between 5 and 8 Hz in stacks of 200–600 images.

Analysis of Exocytosis by TIRFM—Time-sequence stacks of images were manually inspected for rapid brightening of individual spots using the public domain ImageJ software. Exocytotic fusion was defined as a sudden fluorescent burst into the *z* plane followed by dispersal of the signal (34). The fluorescence of each granule was measured as the average intensity in a 1.2 × 1.2-μm region of interest positioned over the center of the granule using the time series analyzer plugin of ImageJ. Net fluorescence intensity was obtained after subtracting the fluorescence background measured outside the cell.

Single Vesicle Tracking and Diffusion Coefficient—Two-dimensional trajectories were obtained from 300-s time lapse TIRFM images using the ImageJ Particle Detector and Tracker plugin. The generated data set contained *x* and *y* coordinates as a function of time. For each vesicle trajectory, the mean square displacement (MSD) in the *xy* plane was calculated based on mathematics described by Steyer and Almers (35) using a self-made script for MATLAB software (The MathWorks). The square displacement between two successive images during a time interval δt was defined by $r^2 = (x_{(t+\delta t)} - x_{(t)})^2 - (y_{(t+\delta t)} - y_{(t)})^2$. The diffusion coefficient D_{xy} was calculated as $D_{xy} = s/4$, with *s* being the slope of the linear fit of the MSD for a given trajectory over a period of time τ.

Gel Electrophoresis and Immunoblotting—Total protein lysates (20 μg/well) or trichloroacetic acid-precipitated proteins were prepared and immunoblotted as described previously (10). The primary antibodies used were as follows: a rabbit polyclonal anti-human SgII (1:2000 in 5% nonfat dry milk (31)); a rabbit polyclonal anti-catestatin (1:500 in 5% nonfat dry milk (36)); a goat polyclonal anti-CgB (C-19, 1:4000 in 5% FBS plus 0.1% Tween 20; Santa Cruz Biotechnology); a mouse monoclonal anti-actin (I-19, 1:500 in 5% FBS plus 0.1% Tween 20; Santa Cruz Biotechnology); or a mouse monoclonal anti-HA antibody (1:1000 in 5% FBS plus 0.1% Tween 20; Covance). Horseradish peroxidase-conjugated secondary antibodies were as follows: a goat anti-rabbit IgG (1:6000 in 5% nonfat dry milk; Bio-Rad); a donkey anti-goat IgG (1:10,000 in 5% FBS plus 0.1% Tween 20; Santa Cruz Biotechnology); or a goat anti-mouse IgG (1:7500 in 5% FBS plus 0.1% Tween 20; Biodesign International). Detection of horseradish peroxidase activity was achieved by chemiluminescence (West Pico, Pierce). Quantitative analysis of immunoreactivity was done with ImageJ software.

Secretion Assay of EAP Chimeras—Cells transfected with the expression plasmids encoding EAP fusion proteins were washed twice with DMEM prior to 30 min of incubation in

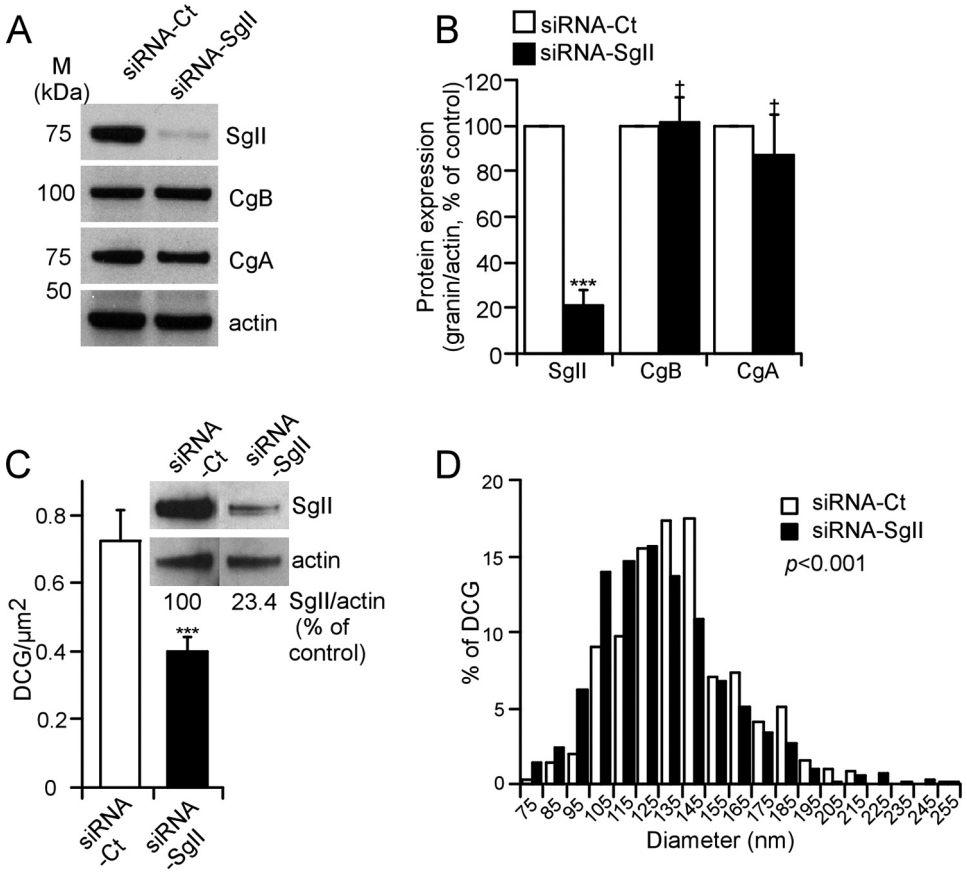

FIGURE 1. **Depletion and altered secretory granule morphology in response to siRNA-mediated silencing of SgII in wild-type sympathoadrenal PC12 cells.** *A,* granins expression. Representative immunoblot of granins expression after siRNA silencing of SgII. Cell lysates from PC12 cells transfected with either siRNA-Ct or siRNA-SgII (96 h) were subjected to immunoblot detection of SgII, CgB, and CgA expression. Actin served as a normalization control. *B,* quantification of relative granin expression. The normalized SgII, CgB, and CgA expression in siRNA-Ct-treated cells was considered to be 100%. Values are given as the mean relative protein expression of seven independent experiments ± S.E. †, $p > 0.05$; ***, $p < 0.001$, *t* test. *C* and *D,* ultrastructural analyses of dense core granules after siRNA silencing of SgII. Micrographs from PC12 cells treated with siRNA-Ct or siRNA-SgII were analyzed for number of dense core granules per μm^2 of cytoplasm (*C*) and diameter (nm) (*D*). $n = 187$ (siRNA-Ct) and 127 (siRNA-SgII) cell planes. *C, immunoblot inset* represents SgII expression before sample processing, quantified as described in *B*. ***, $p < 0.001$, Kruskal-Wallis test. *D,* dense core granule diameters were calculated from 572 (siRNA-Ct) and 586 (siRNA-SgII) randomly selected dense core granules. Values were ranked according to interval, and the distribution of the resulting populations was compared using a Kruskal-Wallis test.

DMEM supplemented or not with A23187. Cell culture supernatants were collected, and cell lysates were prepared by quick freeze/thaw in saline buffer (150 mM NaCl, 5 mM KCl, 2 mM $CaCl_2$, 10 mM HEPES, pH 7.4) containing 0.1% Triton X-100. Detection of EAP enzymatic activity in supernatants and cell lysates was achieved with a high sensitivity chemiluminescence assay (Phospha-Light, Applied Biosystems). The secretion rate of EAP chimeras was calculated as a percentage of the total EAP activity present in the cells before stimulation. Total EAP activity is the sum of the amount released plus the amount remaining in the cells.

Secretion Assay of SgII-HA—A35C-S7 cells stably expressing SgII-HA were extensively washed with DMEM and incubated in DMEM alone for 30 min. Supernatants were collected, and cells were further incubated in DMEM supplemented with 60 mM KCl, 1 μM A23187, or 60 μM nicotine (Sigma) for 30 min prior to final collection of supernatants. Supernatants were cleared by centrifugation (10 min, 4000 × *g*) and concentrated by trichloroacetic acid precipitation. Pellets were processed for gel electrophoresis and immunoblotting.

Sucrose Gradient Fractionation—A postnuclear supernatant from homogenized cells was prepared and subjected to sucrose density gradient fractionation (0.6–2.2 M) as described previously (37). Fractions were collected and assayed for sucrose concentration by refractometry and immunoblotted for HA and CgB immunoreactivity after trichloroacetic acid precipitation.

RESULTS

Down-regulation of SgII Expression by siRNA in PC12 Cells—We designed an siRNA duplex (siRNA-SgII) that specifically targets rat SgII mRNA. Transfection of PC12 cells with siRNA-SgII resulted in a >80% decrease of SgII protein expression as compared with transfection with a control siRNA (*siRNA-Ct*; Fig. 1, *A* and *B*). Decreasing the expression of CgA or CgB *in cella* or *in vivo* may influence the expression of other endogenous granins, including SgII (11, 15, 38). Here we found that SgII silencing does not interfere with the expression of CgA or CgB when compared with siRNA-Ct-treated cells (Fig. 1, *A* and *B*).

Down-regulation of SgII Expression Alters Formation of DCGs in PC12 Cells—Morphometric analyses of DCGs in siRNA-SgII-treated cells *versus* siRNA-Ct-treated PC12 cells were performed at the ultrastructural level by transmission electron microscopy (Fig. 1*C*; visual output not shown). The number of DCG/μm^2 of cytoplasm was 0.72 ± 0.09 in siRNA-Ct-treated PC12 cells (Fig. 1*C*), consistent with DCG abundance in naive PC12 cells (37). In contrast, the number of DCGs was diminished by ~44% (to 0.40 ± 0.04 DCG/μm^2) in response to ~75% reduction of SgII expression (Fig. 1*C*). Although ~97% of DCGs were within a 85–195 nm diameter range in both siRNA-Ct- and siRNA-SgII-treated PC12 cells, the size distribution was shifted to lower values in SgII-silenced PC12 cells (Fig. 1*D*; $p < 0.001$, Mann-Whitney test), resulting in an average diameter of DCGs in siRNA-SgII-treated PC12 cells significantly smaller (131.1 ± 1.2 nm, $n = 572$ granules) than that of control cells (138.9 ± 1.1 nm, $n = 586$ granules). These data reveal a significant contribution of SgII to the formation of DCGs in sympathoadrenal PC12 cells, wherein a reduction in SgII results in a significant decrease in both number and size of DCGs.

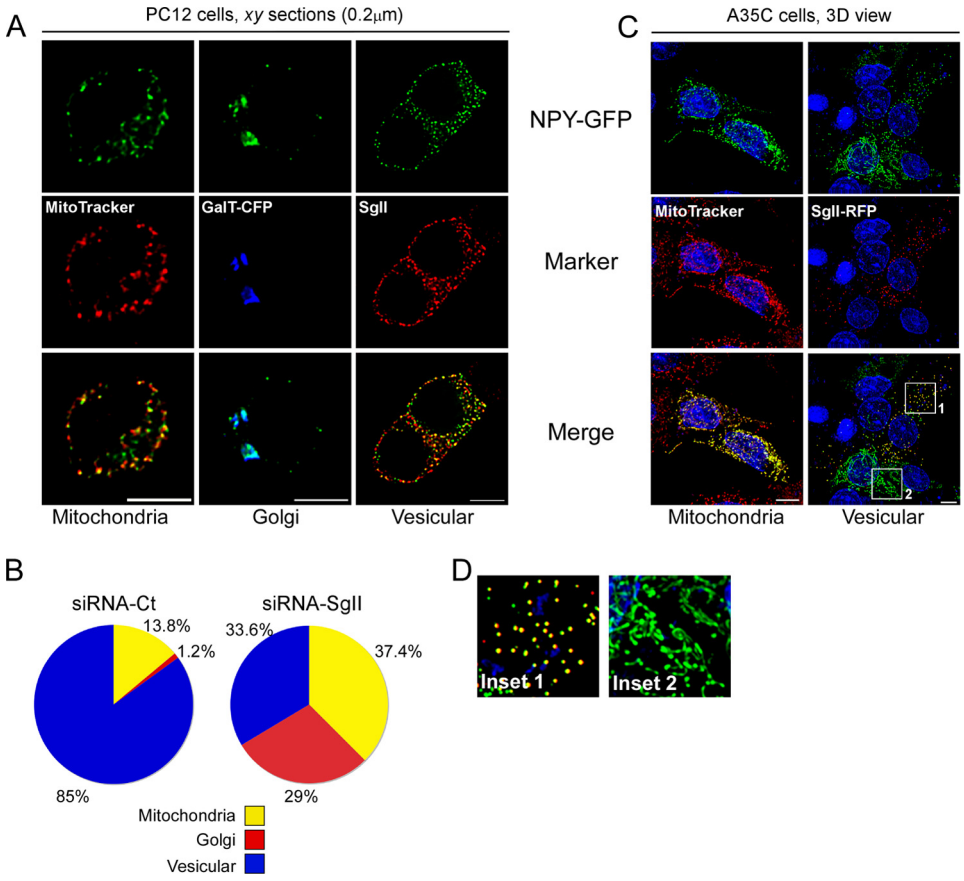

FIGURE 2. **SgII is required for the correct trafficking of NPY-GFP into secretory granules.** *A* and *B*, effect of SgII silencing on secretory granule targeting of NPY in PC12 cells. PC12 cells treated with siRNA-Ct or siRNA-SgII (96 h) were transfected with a plasmid encoding NPY-GFP for 24 h and analyzed by three-dimensional deconvolution microscopy after processing for photoprotein fluorescence and immunocytochemistry. *A*, representative optical *xy* sections of the three archetypal distributions of NPY-GFP observed in PC12 cells. MitoTracker Red CMXros, GalT-CFP, and endogenous SgII were used as markers of mitochondrial, Golgi, or DCG distribution, respectively. *Scale bar*, 5 μm. *B*, relative subcellular distribution of NPY-GFP in control or silenced PC12 cells. The pattern of NPY-GFP localization in transfected cells ($n = 87$, siRNA-Ct; $n = 107$, siRNA-SgII) was classified according to *A*. Values are expressed as a percentage of the number of analyzed cells. $p < 0.0001$, row by column contingency table ($\chi^2 = 58.7$, 2 degrees of freedom). *C* and *D*, expression of SgII reroutes NPY from tubular to vesicular organelles in A35C cells. A35C cells transiently transfected (48 h) with the plasmid encoding NPY-GFP, alone or together with a plasmid encoding SgII-RFP, were processed for photoprotein fluorescence and three-dimensional deconvolution microscopy. *C*, representative three-dimensional (*3D*) views of 9–13 optical *xy* sections acquired along the *z* axis. MitoTracker Red CMXros was used as a marker of the mitochondrial network. Nuclei (*blue*) were visualized with Hoechst 33342. *Scale bars*, 5 μm. Co-localization (*yellow*) of NPY-GFP (*green*) with either mitochondria or SgII-RFP photoprotein (*red*) is shown in the *merged images*. Quantification of fluorescence overlap is reported in the text. *D*, enlarged *insets* from *C* emphasize the punctate co-localization of NPY-GFP in presence of SgII-RFP (*inset 1*) as opposed to the mitochondrial distribution of NPY-GFP in absence of SgII-RFP signal (*inset 2*).

Reduction of SgII Expression Impairs Regulated Secretory Peptide Trafficking into DCGs—The 36-amino acid peptide neurotransmitter NPY is stored in DCGs of neuroendocrine cells (25, 39–41). As expected, transient expression of NPY fused to GFP (NPY-GFP (40)) in PC12 cells resulted in the punctate distribution of the photoprotein in ~85% of the transfected cells (Fig. 2*B*) that substantially co-localized with endogenous SgII (Pearson coefficient $R_p = 0.36 \pm 0.02$, overlap coefficient $R_o = 0.37 \pm 0.02$, $n = 150$ optical sections; Fig. 2*A*). This partial rather than absolute co-localization was consistent with previous reports localizing GFP fusion proteins (SgII-GFP (23) and pro-ANF-GFP (28, 40)) with endogenous markers of DCGs. Two other patterns of distribution of NPY-GFP were observed as follows: (i) a patchy distribution that substantially co-localized with the mitochondrion-selective probe MitoTracker Red CMXRos (13.8% of transfected cells; $R_p = 0.59 \pm 0.03$; $R_o = 0.5 \pm 0.04$, $n = 181$ optical sections; Fig. 2, *A* and *B*), likely resulting from the use of an alternative/internal translation initiation (AUG) site reported to function in mitochondrial targeting of NPY in non-neuroendocrine or secretory-deficient neuroendocrine cells (42–45); and (ii) a juxtanuclear distribution, co-localizing with the TGN-resident glycoprotein β-1,4 galactosyltransferase (GalT-CFP) (1.2% of transfected cells; $R_p = 0.67 \pm 0.03$; $R_o = 0.67 \pm 0.03$; 8 cells, $n = 124$ optical sections; Fig. 2, *A* and *B*), reflecting the incomplete sorting of NPY-GFP at the TGN (37).

Silencing expression of SgII by ~85% markedly altered NPY-GFP targeting to chromaffin DCGs, resulting in only 33.6% of the siRNA-SgII-treated cells showing a vesicular distribution of fluorescence (an ~2.5-fold decrease as compared with control cells; Fig. 2*B*). Moreover, localization of NPY-GFP to mitochondria was increased by ~2.7-fold (37.4% of transfected cells; Fig. 2*B*), although its accumulation within the Golgi compartment was increased by ~24-fold (29% of transfected cells; Fig. 2*B*).

Thus, SgII silencing results in the redistribution of NPY-GFP from DCGs to Golgi and mitochondrial compartments, thereby providing evidence of a contribution of SgII to the formation of a regulated secretory pathway.

SgII Induces the Formation of Vesicular Structures in Neurosecretion-deficient A35C Cells—Consistent with the granulogenic activity of an SgII-Myc fusion protein in several non-neuroendocrine cell types (19), the transient expression of SgII-GFP in COS-7 cells drove the formation of discrete fluorescent punctae (supplemental Fig. S1, *B* and *D*), although expression of the constitutively secreted SIG-GFP (SgII signal peptide SIG fused to GFP (23)) did not (supplemental Fig. S1*A*). Therefore, we used our series of SgII fusion proteins (23) SgII-GFP, SgII-RFP (SgII fused to monomeric RFP), SgII-EAP (SgII fused to EAP) or SgII-HA to characterize the granulogenic activity of SgII in a mutant neuroendocrine cell line. The PC12 cell variant A35C lacks DCGs and a regulated secretory pathway and does not express several DCG proteins, including SgII (10, 46). When expressed in A35C, the constitutively secreted proteins SIG-GFP and SIG-EAP (23)

accumulated within the Golgi complex (Fig. 3*A*), typical behavior of constitutively secreted proteins in sympathoadrenal cells, including A35C cells (supplemental Fig. S2*A*) (10, 23, 28, 37). In sharp contrast, SgII-GFP, SgII-EAP, or SgII-HA displayed a highly punctate distribution throughout the cell body (Fig. 3*A*) and along the entire length and at the termini of neurite-type processes in a subset of A35C cells (Fig. 3*B*). Such a distribution pattern was largely similar to that observed in wild-type PC12 (supplemental Fig. S2*A*) (23) or primary chromaffin cells (23), suggesting storage of the SgII fusion proteins in vesicular organelles with typical DCG trafficking behavior. Turnover of proteins from the constitutive secretory pathway is expected to be rapid because of uninterrupted release, whereas proteins of the regulated secretory pathway are stored and retained for extended periods of time before release (18, 47). PC12 cells expressing the regulated secretory chimera SgII-GFP (23) were exposed to the protein synthesis inhibitor cycloheximide for 3 h to prevent accumulation of newly synthesized proteins (18, 47, 48). In such cells, the punctate distribution of SgII-GFP remained unaffected (supplemental Fig. S2*B*), consistent with storage in DCGs (23). Similarly, a 3-h cycloheximide treatment of A35C cells expressing SgII-RFP did not reduce the punctate distribution of the chimera (Fig. 3*C*), effectively ruling out a potential localization of SgII-RFP in constitutive secretory vesicles and suggesting efficient retention of SgII-RFP within DCG-like structures. In contrast, Golgi accumulation of the constitutively secreted SIG-GFP (23) in both PC12 and A35C cells (supplemental Fig. S2*A* and Fig. 3*A*) completely disappeared after 3 h of cycloheximide treatment (data not shown), consistent with a secretion rate being closely linked to the biosynthesis rate. When A35C cells stably expressing SgII-HA (clonal cell line A35C-S7, see "Experimental Procedures") were next immunostained for the lysosomal/endosomal markers LGP110 and EEA1 (32, 49), there was no co-localization with SgII (Fig. 3*D*), a result observed as well in transiently transfected COS-7 cells (supplemental Fig. S1*C*). Thus, the vesicular structures formed upon adventitious expression of SgII in A35C cells exhibit DCG properties and may not result from storage of the granin within lysosomal/endosomal structures or routing of the protein to the constitutive pathway.

Establishment of a Regulated Secretory Activity and Exocytotic Fusion in A35C Cells—We next tested the competence of SgII-containing vesicles for regulated exocytosis, using the EAP reporter as a highly sensitive way to quantify exocytotic release by chemiluminescence (supplemental Fig. S2*C*) (23, 37, 50). In COS-7 cells, the release of the constitutive secretory protein SIG-EAP was elevated in basal, nonstimulating conditions (7.8 ± 0.6%; Fig. 4*A*, *left*) and only slightly augmented to 0.6-fold over basal in response to the calcium ionophore A23187 (1 μM, 30 min; Fig. 4*A*, *right*). In contrast, nonstimulated secretion of SgII-EAP was low (~1.5%; Fig. 4*A*, *left*), suggesting the efficient retention of the fusion protein. Moreover, A23187 triggered 6.2 ± 0.9% secretion of SgII-EAP into the extracellular medium (4.2-fold increase over basal, $p < 0.001$; Fig. 4*A*, *right*). In the neurosecretory-deficient A35C cells, the secretagogue A23187 (5 μM, 30 min) triggered release of SgII-EAP by 6.9-fold over basal conditions (mock medium; $p < 0.001$; Fig. 4*B*), clearly demonstrating regulated secretion of the chimera. The

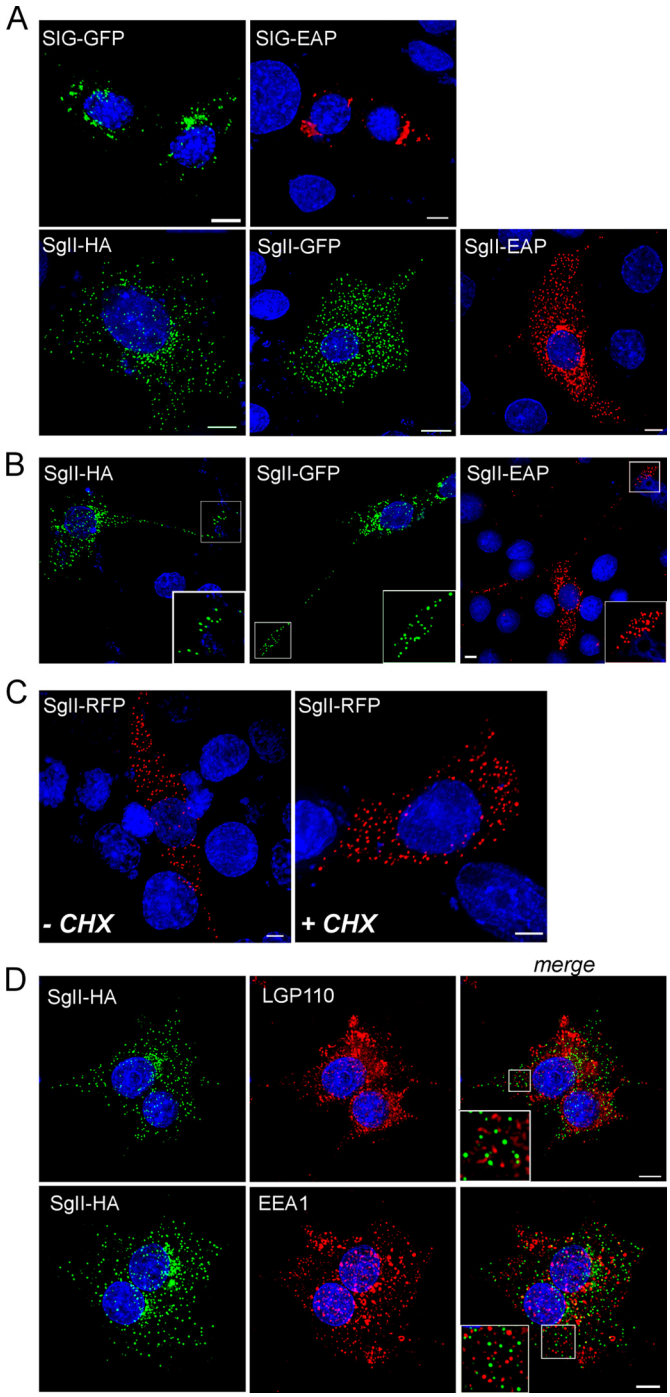

FIGURE 3. **Subcellular distribution of SgII fusion proteins expressed in neurosecretion-deficient sympathoadrenal A35C cells.** A35C cells transfected (48 h) with expression plasmids encoding the indicated fusion proteins were processed for photoprotein fluorescence or immunocytochemistry and three-dimensional deconvolution microscopy. Shown are the three-dimensional views of 9–13 optical *xy* sections acquired along the *z* axis. Nuclei were visualized with Hoechst 33342 (*blue*). SIG-EAP, SgII-EAP (*red*), and SgII-HA (*green*) chimera were detected using the appropriate anti-reporter antibodies. *Scale bars*, 5 μm. *A*, cell bodies. *B*, neurites. Substantial accumulation of SgII-HA/GFP/EAP chimeric proteins is seen at the end of neurite-like structures, as exemplified in the enlarged *insets* of the deconvolved images. *C*, A35C cells expressing SgII-RFP were treated (3 h) with a mock buffer (DMSO; −*CHX*) or the protein synthesis inhibitor cycloheximide (*CHX*) (10 μg/ml; +*CHX*) prior to processing for photoprotein fluorescence. *D*, A35C-S7 cells (stably expressing SgII-HA) were co-stained for SgII-HA (*green*) and the lysosomal/late endosomal marker LGP110 or the early endosomal marker EEA1 (*red*). Absence of co-localization between SgII-HA and lysosomal or endosomal structures is exemplified in the enlarged *insets* from the merged three-dimensional images.

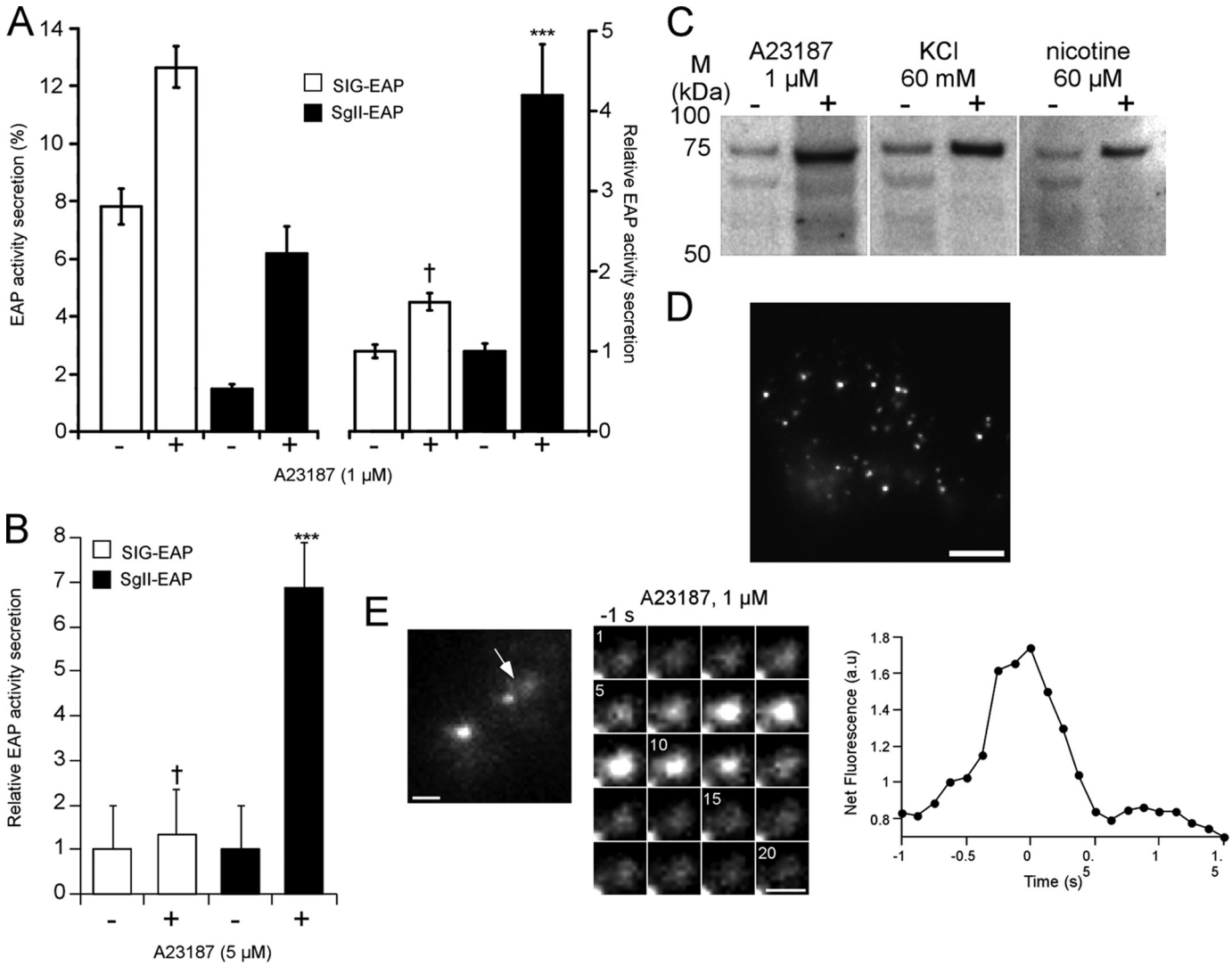

FIGURE 4. **Secretagogue-stimulated exocytosis of SgII in COS-7 and A35C cells.** *A* and *B*, regulated secretion of EAP fusion proteins. COS-7 cells (*A*) and A35C cells (*B*) expressing SIG-EAP or SgII-EAP were exposed for 30 min to DMEM alone (−) or DMEM supplemented with the indicated concentration of A23187 (+). EAP type secretion was assayed as described under "Experimental Procedures." Release of EAP is expressed either as % of EAP activity secretion (*A, left*) or relative to enzymatic activity released in the absence of secretagogue (*A, right,* and *B*). Values are given as the mean ± S.E. of triplicate determinations. Results from one of at least three independent experiments are shown. †, $p > 0.05$; ***, $p < 0.001$, as compared with control, analysis of variance with Dunnett's post-hoc test. *C,* stimulated release of SgII-HA from A35C-S7 cells. A35C-S7 cells were sequentially exposed for 30 min to DMEM (−) and then DMEM containing the indicated secretagogues (+). The resulting supernatants were subjected to immunoblotting. The amount of secreted SgII-HA was quantified by densitometry in three independent secretion experiments. The means ± S.E. of fold increases in stimulated (+) over basal (−) conditions were as follows: A23187, 5.9 ± 1.2; KCl, 4.8 ± 0.8; nicotine, 4.9 ± 1.7. *D,* TIRFM image of a characteristic A35C cell expressing SgII-GFP. Only the pool of vesicles within ~140 nm from the plasma membrane in the *z* axis (corresponding to the estimated penetration depth of the evanescent wave used to excite GFP) is seen. *Scale bar,* 5 μm. *E,* secretagogue-evoked release of SgII-GFP observed by TIRFM. The *arrow* in the overall view of a transfected A35C cell prior (−1 s) to stimulation with 1 μm A23187 (*left*) indicates the exocytotic event depicted in the adjacent sequential images. Shown on the *right* is the quantification of the fluorescence intensity changes measured from the sequential images.

release of SgII-EAP was lower than that typically observed in PC12 cells (supplemental Fig. S2*C*) (23) but significantly higher than the release of SIG-EAP, which showed no response to A23187 ($p > 0.05$; Fig. 4*B*).

Additional insight into the regulated secretory profile of SgII was obtained from the clonal cell line A35C-S7 (stably expressing SgII-HA, see "Experimental Procedures"). As expected, exposure of A35C-S7 cells to A23187 (1 μM, 30 min) stimulated release of SgII immunoreactivity (5.9 ± 1.2-fold over basal, $p < 0.001$; Fig. 4*C*). In addition, membrane depolarization (by 60 mM KCl) or stimulation of the physiological (nicotinic-cholinergic) secretory pathway by nicotine (60 μM) triggered significant release of SgII immunoreactivity in the extracellular milieu by 4.8 ± 0.8- and 4.9 ± 1.7-fold over basal, respectively ($p < 0.001$; Fig. 4*C*). Thus, release of SgII from A335C cells may be triggered not only by creating artificial Ca^{2+} pores but also by secretagogues known to selectively activate cell surface Ca^{2+} channels in neurosecretory cells.

We further examined the exocytotic fusion behavior of single vesicles containing SgII-GFP in A35C cells by TIRFM, which takes advantage of a laser-induced evanescent wave to selectively excite fluorophores in the region adjacent to the glass interface (34). Consistent with wide field fluorescence microscopy results (Fig. 3), we observed a pool of SgII-GFP-containing vesicles within ~140 nm of the plasma membrane of transfected A35C (Fig. 4*D*). Exposure to A23187 (1 μM) caused a

fluorescent burst into the *z* plane from a few discrete vesicles at the plasma membrane, followed by a rapid dispersal of the signal within 500 ms (Fig. 4*E*). This behavior, although observed less frequently than in PC12 cells, is characteristic of an exocytotic event (34) releasing SgII-GFP from the vesicle core, causing granular deprotonation and dequenching of the fluorescence of GFP as the fusion pore expands into the plasma membrane. Taken together, these results clearly demonstrate that the expression of SgII in neurosecretion-deficient A35C re-induces a regulated secretory activity in the cells.

SgII Reroutes NPY Trafficking from Mitochondrial Compartments into Secretory Granules in A35C Cells—When expressed in A35C cells, NPY-GFP consistently displayed a branched, reticular distribution that co-localized with MitoTracker Red CMXRos ($R_p = 0.76 \pm 0.03$ and $R_o = 0.77 \pm 0.03$; Fig. 2, *C* and *D, inset 2*), consistent with previous studies documenting mitochondrial targeting of NPY in secretory-deficient neuroendocrine cells (42–45). In sharp contrast, A35C cells co-expressing NPY-GFP and SgII-RFP consistently showed a highly punctate distribution and substantial co-localization of the two fluorescent signals ($R_p = 0.61 \pm 0.04$ and $R_o = 0.61 \pm 0.04$; Fig. 2, *C* and *D, inset 1*). Thus, the expression of SgII in A35C cells rescues the trafficking of NPY into SgII-containing DCGs.

Morphology and Physical Properties of SgII-containing Vesicles in A35C Cells Reveal Metrics Similar to Those of Genuine DCGs—The morphology of the vesicular structures formed upon SgII expression was first assessed by fluorescence microscopy (Fig. 3*A*). In SgII-GFP-expressing A35C cells, the average apparent diameter of fluorescent punctae was 290 ± 1.2 nm, similar to the 310 ± 2.5 nm diameter of SgII-GFP-labeled DCGs in normal PC12 cells (23). Examination by immunoelectron microscopy of A35C-S7 cells revealed electron dense, membrane-bound vesicles (Fig. 5*A*) with an average diameter (133.2 ± 6.8 nm) within the same range as that of chromaffin DCGs (138.9 ± 1.1 nm, Fig. 1*D*) (53). The resolution of fluorescence puncta is diffraction-limited, and our measure of granule diameter by light microscopy is, as expected, an overestimation of the actual size of the granules that is more accurately estimated by electron microscopy. We note that our estimation of DCG size by fluorescence microscopy is consistent with earlier reports from us and others estimating the diameter of fluorophore-labeled DCGs (23, 51, 52, 54). Accumulation of SgII within the dense core area of the granules was confirmed by the presence of HA-labeling 10 nm gold particles (Fig. 5*A*). No such structures could be found in either naive A35C cells (10, 27) or A35C cells stably transfected with the corresponding control plasmid (pcDNA3.1/Hygro(+) vector; data not shown).

We next performed equilibrium sucrose density gradient fractionation on post-nuclear supernatants prepared from a sample combining both A35C-S7 and PC12 cells (Fig. 5, *B* and *C*). Immunoreactivity for HA was used to identify A35C vesicles, whereas endogenous CgB immunoreactivity specifically localized PC12 DCGs along the gradient. SgII-HA co-localized with CgB in the same fractions, with maximum immunoreactivity at 1.24 M sucrose (Fig. 5*C*), consistent with the known buoyant density of DCGs isolated from PC12 cells (28, 37). Thus, expressing SgII in A35C cells results in the formation of

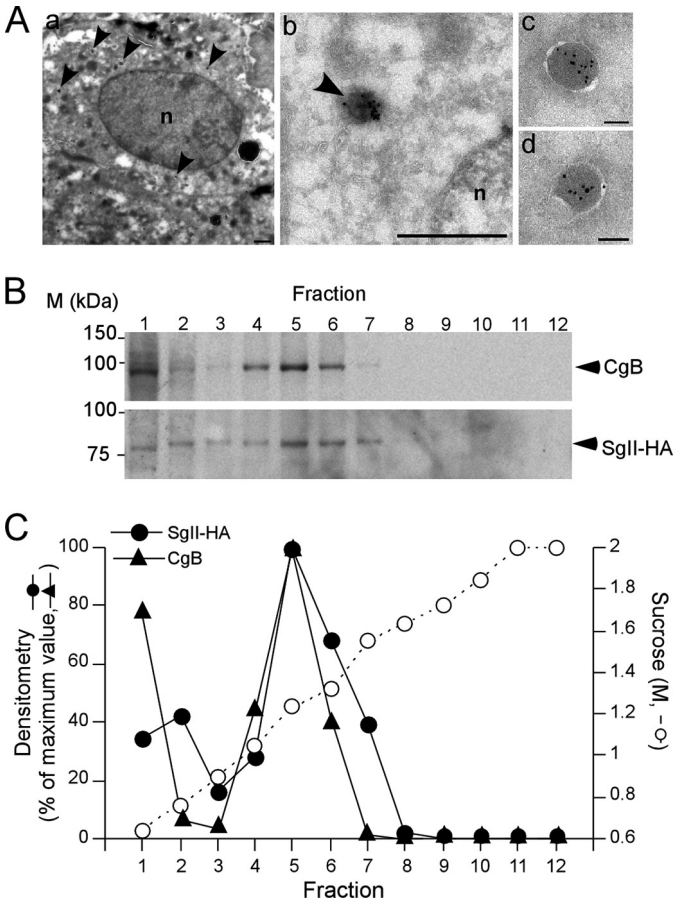

FIGURE 5. **Morphometric analyses of SgII-containing dense core granules in A35C cells.** *A,* immunoelectron microscopy analysis of A35C-S7 cell line. SgII-HA was detected using a monoclonal anti-HA antibody and a secondary 10 nm gold-conjugated goat anti-mouse antibody. *Panels a* and *b,* newly formed granules are indicated by the *arrowheads. Scale bars, a*, 1 μm; *b*, 200 nm. *Panels c* and *d,* detailed structure of SgII-containing vesicles. *Scale bars,* 100 nm. *B* and *C,* buoyant density of dense core secretory granules from PC12 and A35C-S7. Postnuclear supernatants from a mixed population of PC12 and A35C-S7 cells were subjected to a sucrose density gradient fractionation. *B,* immunoblots of CgB (from PC12) and SgII-HA (from A35C-S7) distribution across the sucrose density gradient. *C,* quantification of CgB and SgII-HA amounts in the gradient fractions from *B*. Values are given as the percent maximum of either CgB or SgII-HA signal in the gradient fractions.

dense core vesicles with morphological and physical properties largely similar to that of *bona fide* DCGs.

Dynamics of Single SgII-containing Vesicles in Living A35C Cells—We next compared the mobility of SgII-GFP-containing granules between A35C and PC12 cells in resting conditions (Fig. 6). The MSD from ~150 SgII-containing vesicles in each cell type (see "Experimental Procedures") was determined from tracking analyses (Fig. 6, *A* and *B*). When plotted against time (Fig. 6*C*), MSDs from A35C and PC12 cells exhibited a linear distribution, characteristic of random diffusion of the vesicles. The distribution pattern of the diffusion coefficients was virtually identical between the two cell types ($p > 0.05$, Mann-Whitney test; Fig. 6*D*), with more than 82% of the vesicles within the $5–45 \cdot 10^{-4}$ $\mu m^2 \cdot s^{-1}$ D_{xy} range, indicating similar motion of SgII-containing granules in resting A35C and PC12 cells.

Acidic Environment Is a Prerequisite for the Secretory Granule Forming Activity of SgII in A35C Cells—We previously reported the requirement of a pH gradient along the secretory

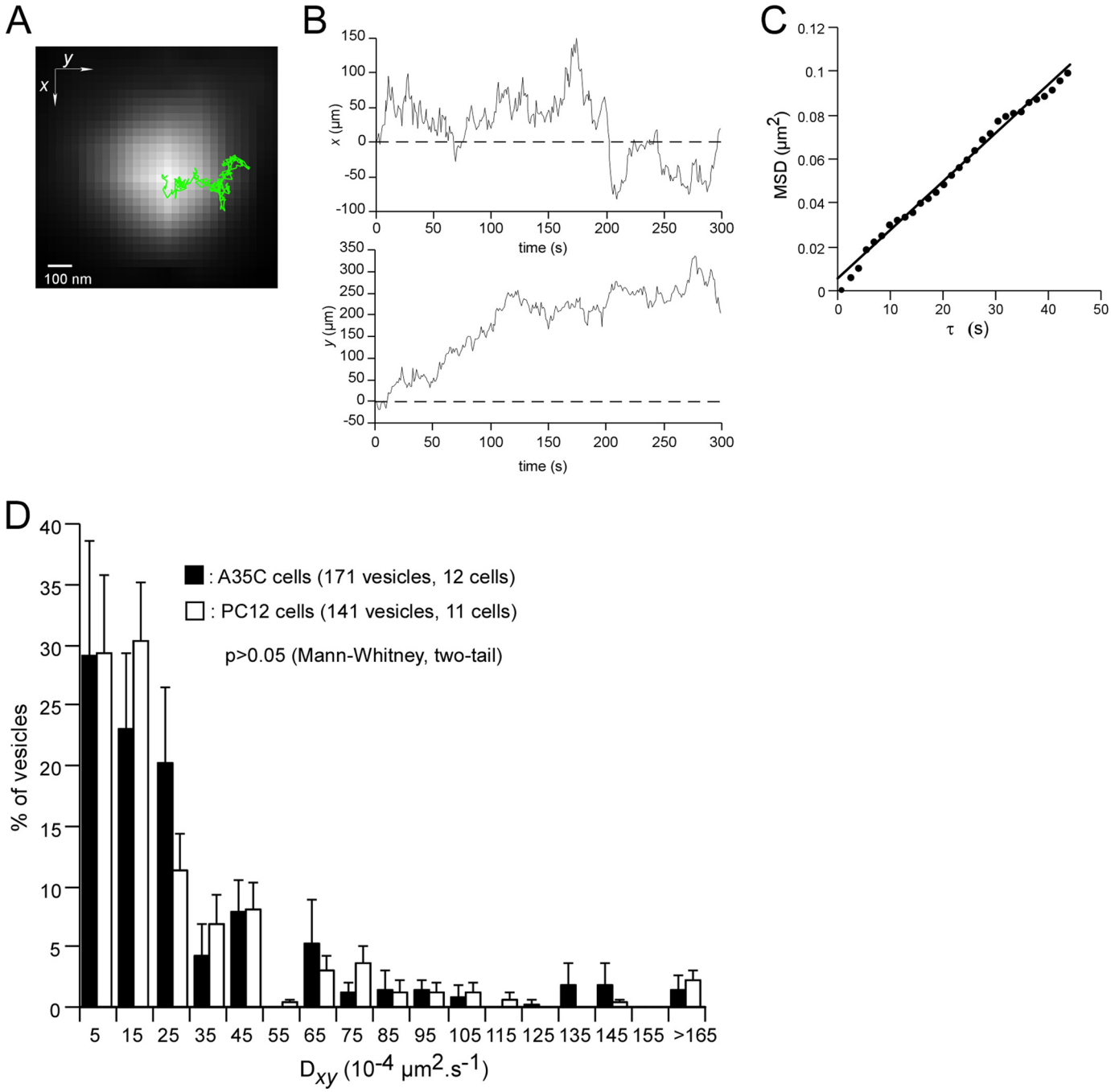

FIGURE 6. **Mobility of secretory vesicles is comparable in A35C expressing SgII-GFP cells and wild-type PC12 cells.** *A,* TIRFM image of a characteristic SgII-GFP-containing granule in a transfected A35C cell. The granule trajectory in the *xy* plane (*green line*) over a period of 300 s was used to generate *x* and *y* coordinates and calculate the MSD and diffusion coefficient values. *Scale bar,* 100 nm. *B, x* and *y* coordinates extracted from *A* as a function of time. *C,* MSD from the origin as a function of time obtained from *B*. *D,* mobility of SgII-containing granules in SgII-GFP-expressing A35C *versus* PC12 cells. Diffusion coefficients (D_{xy}) values from 171 vesicles in 12 A35C cells and 141 vesicles in 12 PC12 cells were ranked according to histogram intervals and compared using a Mann-Whitney two-tail test.

pathway for the formation of CgA-containing DCGs in PC12 cells (37). Chronic exposure (22 h) of SgII-GFP-expressing PC12 cells to a low dose (10 nM) of the selective V-ATPase inhibitor BafA1 resulted in a reduced number of DCGs positive for SgII-GFP (supplemental Fig. S2*D*), which underscores the importance of V-ATPase-mediated acidification of late compartments of the secretory pathway for granulogenesis. Thus, we questioned whether the SgII-mediated biogenesis of secretory vesicles would also require functional V-ATPases in A35C cells, and we assessed the effect of chronic exposure of transfected A35C cells to BafA1 (Fig. 7, *A* and *B*). Although control (mock-treated) A35C cells showed an average fluorescent vesicle density (number of green punctae/μm^2 of cell body) of 0.15 ± 0.02, that of A35C cells exposed to BafA1 was down to 0.09 ± 0.01, corresponding to an ~40% decrease in vesicle density ($p < 0.05$, *t* test; Fig. 7*A*). In the same conditions (Fig. 7*B*), exposure of SgII-EAP-expressing A35C cells to BafA1 resulted in an ~20% reduction of regulated, A23187-evoked secretion of

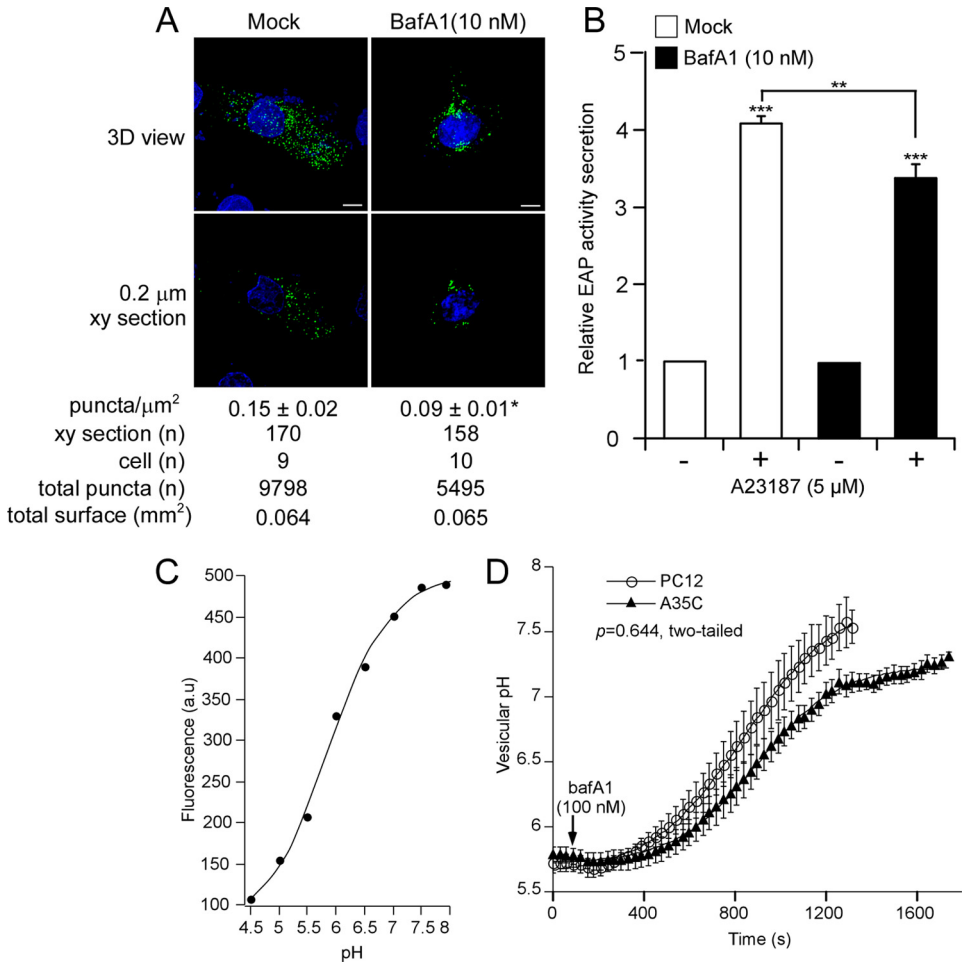

FIGURE 7. **Effects of the vacuolar H^+-V-ATPase inhibitor BafA1 on the granule forming activity of SgII and the regulation of pH_{ves} in SgII-expressing A35C cells.** *A,* subcellular distribution of SgII-GFP in A35C cells treated with BafA1. A35C transfected with SgII-GFP and exposed (22 h) to mock (DMSO) or BafA1 (10 nM) were analyzed by deconvolution microscopy. Shown are representative three-dimensional (*3D*) images or *xy* section (0.2 μm) views. Nuclei were visualized with Hoechst 33342 (*blue*). *Scale bars,* 5 μm. *, $p < 0.05$, *t* test. *B,* secretagogue-evoked release of SgII-EAP after BafA1 treatment. A35C cells transfected with SgII-EAP and exposed (22 h) to mock (DMSO) or BafA1 (10 nM) were subjected to a 30-min exposure to DMEM alone (−) or DMEM supplemented with 5 μM A23187 (+) and assayed for EAP secretion. The release of EAP is expressed relative to enzymatic activity released in the absence of secretagogue. Values are given as the mean ± S.E. of three independent experiments, each done in triplicate. **, $p < 0.005$; ***, $p < 0.001$, as compared with control, analysis of variance with Bonferroni's post hoc test. *C,* representative pH titration curve of SgII-GFP fluorescence. a.u., arbitrary units. *D,* effect of BafA1 on pH_{ves} in A35C *versus* PC12 cells. PC12 and A35C cells ($n = 5$) expressing SgII-GFP were exposed to 100 nM BafA1. Fluorescence was monitored every 30 s over a 20-min period, and algebraic conversion of GFP fluorescence to pH values was obtained as described under "Experimental Procedures," using the pH titration curve shown in *C*. Values are given as the mean ± S.E. Kinetics of pH increase were compared using a Mann-Whitney two-tail test.

the chimera as compared with control cells ($p < 0.01$; Fig. 7*B*). Therefore, V-ATPase acidification of the engendered secretory pathway in A35C cells is required for the DCG forming activity of SgII.

Regulation of Secretory Granule Intravesicular pH (pH_{ves}) in Living A35C Cells—We next aimed at investigating the status of pH_{ves} in SgII-GFP-containing granules in A35C cells (Fig. 7, *C* and *D*). As anticipated, titration of SgII-GFP fluorescence *in cella* revealed strong sensitivity to pH with an apparent pK_a of 6.34 ± 0.04 and a Hill coefficient of 0.9 ± 0.03 (Fig. 7*C*). Consistent with the known acidic pH of chromaffin granules (55), the pH_{ves} of PC12 was 5.78 ± 0.06 (Fig. 7*D*). A similar acidic pH_{ves} was observed in A35C (5.72 ± 0.07; Fig. 7*D*), suggesting functional V-ATPases in the newly formed SgII-containing granules. To test this hypothesis, transfected A35C and PC12 cells were further exposed to an acute dose of BafA1 (100 nM), and single cell fluorescence response was monitored over time. As shown in Fig. 7*D*, exposure to BafA1 provoked a rapid alkalinization of SgII-containing granules in both PC12 and A35C cells, ultimately leading to the equilibration of pH_{ves} with cytoplasmic pH values (PC12, 7.53 ± 0.13; A35C, 7.11 ± 0.07; Fig. 7*D*). Kinetics of such alkalinization were similar between PC12 and A35C cells ($p > 0.05$, Mann-Whitney two-tail test; Fig. 7*D*), confirming that the SgII-containing granules in A35C cells contain functional V-ATPases maintaining the acidic luminal pH characteristic of *bona fide* DCGs.

Plasma Membrane Depolarization Induces Alkalinization of Secretory Granule Core in PC12 and A35C Cells—In PC12 cells, depolarization of the plasma membrane results in a rapid, calcium-dependent alkalinization of the DCG core prior to exocytosis (56). We thus questioned whether this phenomenon could be observed in A35C cells as well (Fig. 8). As expected, superfusion of PC12 cells expressing SgII-GFP with 50 mM KCl induced an initial rapid fluorescence increase (~110%; Fig. 8*A*), corresponding to vesicle alkalinization before exocytosis (56) followed by a slow fluorescence decrease, indicative of peptide release by exocytosis (Fig. 8*A*) (56). Accordingly, when botulinum C1 light chain (L-BoNT/C1), a blocker of late soluble NSF attachment protein receptor-mediated steps in exocytosis (10), was co-expressed with SgII-GFP, the initial alkalinization phase was followed by a sustained increase in fluorescence (~200%, Fig. 8*A*), indicating the retention of SgII-GFP inside the granules due to impaired formation of the exocytotic pore. However, the absence of Ca^{2+} outside (+EGTA) or inside (+BAPTA/AM) PC12 cells failed to prevent the rapid alkalinization phase in our conditions (Fig. 8*A*) (56). No fluorescence variations were observed when vehicle was added instead of KCl (Fig. 8*A*), demonstrating the specificity of the response to the depolarization process.

When A35C cells expressing SgII-GFP were subjected to membrane depolarization with 50 mM KCl, SgII-GFP fluorescence exhibited the same initial rapid increase (110%; Fig. 8) as

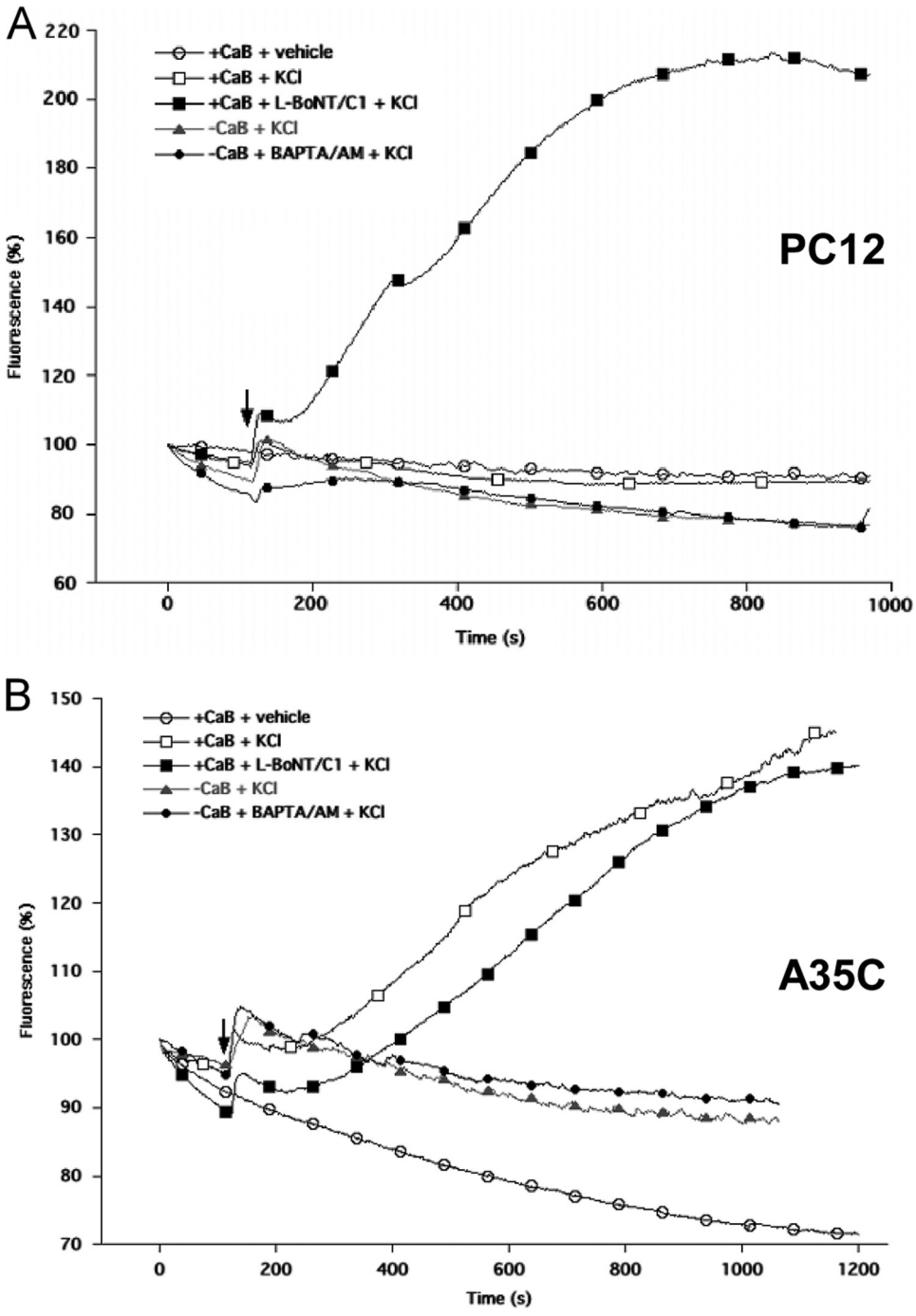

FIGURE 8. **KCl depolarization induces alkalinization of SgII-GFP-containing granules in PC12 and A35C cells.** Kinetics of fluorescence changes following KCl depolarization in PC12 cells (*A*) or A35C cells (*B*) expressing SgII-GFP alone or together with botulinum neurotoxin C1 light chain (+*L-BoNT/C1*). Cells were preincubated for 10 min in either a calcium-containing buffer (+*CaB*), a calcium-depleted buffer (−*CaB*), or a calcium-depleted buffer containing 50 mM of BAPTA/AM (−*CaB* + *BAPTA/AM*). Whole cell fluorescence was continuously monitored (500-ms acquisition frames) over a 20-min period. Superfusion of 50 mM KCl (+*KCl*) or H_2O (vehicle) was performed at the indicated time (*black arrow*). Changes in fluorescence are expressed as a percentage of the fluorescence present in the cell before superfusion. Measurements were done in triplicate for each cell type, in at least three independent experiments. Shown are the kinetics of one typical transfected cell.

in PC12 cells (Fig. 8*A*). However, it was followed by a slow and sustained fluorescence rise (140%; Fig. 8*B*), similar to that of L-BoNT/C1 co-expressing PC12 (Fig. 8*A*) or A35C (Fig. 8*B*), and therefore reminiscent of impaired formation of the fusion pore. Although the initial alkalinization phase in A35C was Ca^{2+}-independent (Fig. 8*B*) as in PC12 cells (Fig. 8*A*), Ca^{2+} depletion in A35C cells abolished the second phase of the response (Fig. 8*B*).

DISCUSSION

Overview—In this study, we aimed at characterizing the role of SgII in the biogenesis of DCGs of sympathoadrenal chromaffin cells. Although this secretory protein has been extensively used as a marker of the regulated secretory pathway (53, 57, 58), its function in the formation of DCGs has not been carefully investigated, and so far it remains elusive (19, 22). By analyzing the consequences of SgII down-regulation in the neuroendocrine PC12 cell line, and its ability to rescue a regulated secretory pathway in the secretory-deficient PC12 variant A35C, we demonstrate the importance of SgII for DCG biogenesis in neuroendocrine cells and characterize fundamental features of SgII-mediated granulogenesis.

SgII as Necessary Factor in the Formation of DCGs in PC12 Cells—Unlike results from CgA knock-out mice reporting concomitant changes in CgB and SgII expression (14, 15, 38), the down-regulation of SgII expression in isolated PC12 cells did not alter the expression levels of CgA and CgB (Fig. 1). In line with studies addressing CgA- or CgB-mediated granulogenesis in model cell lines (11, 12, 47), our results emphasize the necessity of *in cella* analyses to assess the direct role of granins in the regulation of DCG formation. We found a disproportion between the degree of silencing of SgII expression and the decreased number of DCGs in PC12 cells (~80% *versus* ~40%; Fig. 1); such disproportion has been reported for CgA and CgB silencing effects as well (10–12). This substantiates the concept of granulogenic redundancy, which may now be broadened to the three major granin family members.

What is the catecholamine metabolism status in PC12 cells lacking SgII? Uptake, storage, and exocytotic release of catecholamines are impaired in CgA-deficient mice (14, 38, 59), perhaps because of the combined absence of catecholamine

binding/concentration properties of CgA (60) and the lower catecholamine affinity of the remaining cargo proteins, including SgII (38). Although additional experiments are required to further characterize the relationships between SgII and catecholamine metabolism, its necessary role for DCG formation in sympathochromaffin cells described in this study creates a convincing mechanistic link for the previously observed association between quantitative genetic variation at the *SCG2* locus and human hypertension (2).

Prototype secretory proteins with a trafficking fate dependent on the presence/absence of a regulated secretory pathway (*e.g.* constitutively secreted or mis-trafficked to the lysosomal pathway in secretory-deficient variants) include human growth hormone, the bovine pro-hormone pro-opiomelanocortin, and carboxypeptidase H (10, 12, 27, 61). Here, we used NPY, routed to the mitochondria in non-neuroendocrine and secretory-deficient neuroendocrine cells (42–45), as a prototype secretory protein. The substantial re-localization of NPY-GFP (25) in SgII-depleted PC12 cells and rescued A35C cells (Fig. 2) clearly emphasizes the chaperone function of SgII for NPY trafficking during DCG biogenesis. Of note, the initial characterization of the A35C cell line reported a then inexplicable mitochondrial morphology variation (27) that might now be linked to the mitochondrial re-localization of endogenous NPY.

SgII Can Rescue the Formation of DCGs and a Regulated Secretory Activity in A35C Cells—Taking our cue from the experimental paradigm developed in our earlier studies on SgII trafficking (23) and CgA-mediated granulogenesis in sympathoadrenal cells (10), we assessed the ability of SgII to rescue the formation of functional DCGs (47, 62) in the secretory-deficient PC12 variant A35C. We conclude from our results (Figs. 3 and 5) that the morphological parameters defining a DCG (63) are met when SgII is expressed in A35C cells. Similar outcomes are obtained upon expression of CgA in secretory-deficient endocrine cells lines (10, 12). However, expression of CgA, CgB, or SgII in non-neuroendocrine cells consistently generates larger vesicular structures than PC12 DCGs (11, 17, 19). Secretory-deficient PC12 variants may therefore be higher fidelity cellular models to understand the neurosecretion competence (46, 64).

A *sine qua none* characteristic of functional secretory granule is the ability to store and release its cargo upon stimulation (10, 12, 19, 46, 62). Our complementary secretion approaches clearly establish the exocytotic release of SgII triggered by exposure of rescued A35C cells to secretory stimuli (Fig. 4) and provide evidence for the efficient retention of SgII under basal conditions both in A35C and COS-7 cells. However, our kinetic results on DCG alkalinization in response to plasma membrane depolarization (Fig. 8) suggest that a less efficient exocytotic process leads to intracellular accumulation of secretion-incompetent granules, perhaps due to limited recovery of soluble NSF attachment protein receptors deficiencies in A35C cells. Accordingly, we noticed a modest exocytosis frequency of SgII-GFP in transfected A35C measured by TIRFM (Fig. 3*E*), as compared with that of Vamp-GFP or NPY fusion proteins in bovine chromaffin or PC12 cells (41, 65),[5] as well as a systematically lower steady-state regulated release of SgII in A35C as compared with PC12 cells (Fig. 3*B* and supplemental Fig. S2*C*) (23). Also, the average density of SgII-GFP-containing granules in transfected A35C cells was lower than that of transfected PC12 cells (0.15 ± 0.09 punctae per μm^2 *versus* 0.91 ± 0.07 punctae per μm^2, see Fig. 7*A* and supplemental Fig. S2*B*). A similar conclusion may be drawn from our CgA studies (10, 37) and from CgB- or SgII-regulated secretion in non-neuroendocrine cell lines (11, 19). Despite the moderate efficiency of SgII to establish an otherwise *bona fide* neurosecretory phenotype, the strength of the mutant A35C cell model lies in its ability to implement a minimalistic yet robust approach to study basic mechanisms that underlie the granulogenic role of SgI in a cellular system of neuroendocrine origin in the absence of a putative compensatory effect from other granins.

Most of the intrinsic properties of SgII-containing DCGs in living A35C cells analyzed in this study point toward a substantial homology with genuine SgII-GFP-containing DCGs in PC12 cells (Figs. 6–8) (35, 56, 66). Rescued A35C cells may therefore contain the minimal machinery necessary for the formation of mature DCGs via a typical and functional maturation process (53), including acidification of immature secretory granule core through the proton pump V-ATPase (55), transport toward the plasma membrane (67), and transduction of a signal for intragranular pH rise in response to plasma membrane depolarization. A chromaffin granule membrane Na^+/H^+ antiporter activity (68) may contribute to changes in granule core cation concentrations during stimulation (69), as well as a Ca^{2+}-independent, high conductance K^+-selective granule membrane channel (70). Further experiments, *e.g.* proteomic analyses, will be needed to specify the exact composition of SgII-containing DCGs in rescued A35C cells and further dissect the protein machineries present in newly formed secretory granules.

Granulogenic Role of SgII, Mechanism, Hypothesis, and Future Directions—What are the mechanisms underlying the granulogenic function of SgII? We propose that SgII acts through aggregation to initiate the physical driving force required for vesicle budding at the TGN. Granins undergo acidic pH- and Ca^{2+}-dependent aggregation *in vitro* (6, 7, 60) and *in cella* (5), and predicted coiled-coil secondary conformations may enable their very dense packaging within secretory granules (59). Sorting of SgII into the regulated secretory pathway of PC12 requires an acidic environment (57) and relies on a saturable mechanism at the TGN (23). A V-ATPase-mediated acidification of the secretory pathway is known to be necessary for DCG biogenesis in several neuroendocrine cell types (37, 71, 72), and expression of aggregation-competent regulated cargo proteins is sufficient for granule-like formation in non-neuroendocrine cells (11, 12, 17, 19, 73). Here, using the secretory-deficient A35C cells, we specifically establish the V-ATPase-dependent granule forming activity of SgII (Fig. 7), sustaining the hypothesis that SgII aggregates pioneer the formation of secretory granules.

Because inhibition of the V-ATPase activity partially abolishes SgII granulogenic activity in rescued A35C cells (Fig. 7), additional *trans*-determinants may contribute to DCG formation at the TGN. For instance, SgII, CgA, and CgB are known to

[5] M. Courel, D. T. O'Connor, and L. Taupenot, unpublished results.

interact with vesicle membranes at acidic pH (7, 74, 75), and specific binding partners for CgA at the TGN have been identified, including the granin family member SgIII (76–79) and the Golgi-resident proteins of the stathmin family SCLIP and SCG10 (61). Interaction between CgA and SgIII involves the amino-terminal α-helical structure CgA-(48–111) (78), which contains both a necessary sorting domain in PC12 cells (28) and a granulogenic determinant in A35C and COS-1 cells (10, 18). SgIII interacts *in cella* with SgII in pituitary cells (80) but not in PC12 (78). Down-regulation of SCLIP expression alters the trafficking of SgII in PC12 (61), although a direct interaction between SgII and SCLIP has yet to be determined. Considering the secondary structure findings pertaining to CgA (10, 18, 28), we propose that the two small α-helical sorting domains of SgII (23) will be of interest for both *cis*- and *trans*-determinant mechanisms mediating SgII granulogenic activity.

The granulogenic function of SgII might result as well from a more widespread, overall regulatory effect of the granin. Indeed, the characterization of secretory-deficient variants of PC12 cells points to alterations in transcriptional control of the regulated secretory pathway (46, 64, 81), and a post-translational regulatory mechanism mediated by the protease inhibitor protease Nexin-1 is proposed to account for the granulogenic role of CgA in pituitary 6T3 cells (12, 82, 83). How silencing of SgII in PC12 cells affects the expression of other crucial components of the DCG and whether such proteins are synthesized *de novo* by rescued A35C cells remain to be discovered. CgB may be present in the nuclei of chromaffin cells and rat cardiomyocytes where it could have a regulatory effect on gene expression (84, 85). Of note, SgII reportedly co-localizes with CgB in the nuclei of PC12 cells (86), and the SgII-derived peptide manserin has been detected as well in nuclei of rat duodenal villus cells (87).

Acknowledgments—We appreciate the technical assistance of Timo Meerloo during the immunoelectron microscopy (laboratory of Marilyn Farquhar, University of California, San Diego). Digital imaging was performed at the Cancer Center Shared Resource Facilities (University of California, San Diego) and at the National Center for Microscopy and Imaging Research CMIR (funded in part by grants from the National Institutes of Health).

REFERENCES

1. Chen, Y., Rao, F., Rodriguez-Flores, J. L., Mahata, M., Fung, M. M., Stridsberg, M., Vaingankar, S. M., Wen, G., Salem, R. M., Das, M., Cockburn, M. G., Schork, N. J., Ziegler, M. G., Hamilton, B. A., Mahata, S. K., Taupenot, L., and O'Connor, D. T. (2008) *J. Am. Coll. Cardiol.* **52,** 1468–1481
2. Wen, G., Wessel, J., Zhou, W., Ehret, G. B., Rao, F., Stridsberg, M., Mahata, S. K., Gent, P. M., Das, M., Cooper, R. S., Chakravarti, A., Zhou, H., Schork, N. J., O'connor, D. T., and Hamilton, B. A. (2007) *Hum. Mol. Genet.* **16,** 1752–1764
3. Morvan, J., and Tooze, S. A. (2008) *Histochem. Cell Biol.* **129,** 243–252
4. Taupenot, L., Harper, K. L., and O'Connor, D. T. (2003) *N. Engl. J. Med.* **348,** 1134–1149
5. Chanat, E., and Huttner, W. B. (1991) *J. Cell Biol.* **115,** 1505–1519
6. Gerdes, H. H., Rosa, P., Phillips, E., Baeuerle, P. A., Frank, R., Argos, P., and Huttner, W. B. (1989) *J. Biol. Chem.* **264,** 12009–12015
7. Park, H. Y., So, S. H., Lee, W. B., You, S. H., and Yoo, S. H. (2002) *Biochemistry* **41,** 1259–1266
8. Yoo, S. H., and Lewis, M. S. (1996) *J. Biol. Chem.* **271,** 17041–17046
9. Gorr, S. U., Dean, W. L., Radley, T. L., and Cohn, D. V. (1988) *Bone Miner.* **4,** 17–25
10. Courel, M., Rodemer, C., Nguyen, S. T., Pance, A., Jackson, A. P., O'connor, D. T., and Taupenot, L. (2006) *J. Biol. Chem.* **281,** 38038–38051
11. Huh, Y. H., Jeon, S. H., and Yoo, S. H. (2003) *J. Biol. Chem.* **278,** 40581–40589
12. Kim, T., Tao-Cheng, J. H., Eiden, L. E., and Loh, Y. P. (2001) *Cell* **106,** 499–509
13. Kim, T., Zhang, C. F., Sun, Z., Wu, H., and Loh, Y. P. (2005) *J. Neurosci.* **25,** 6958–6961
14. Mahapatra, N. R., O'Connor, D. T., Vaingankar, S. M., Hikim, A. P., Mahata, M., Ray, S., Staite, E., Wu, H., Gu, Y., Dalton, N., Kennedy, B. P., Ziegler, M. G., Ross, J., and Mahata, S. K. (2005) *J. Clin. Invest.* **115,** 1942–1952
15. Hendy, G. N., Li, T., Girard, M., Feldstein, R. C., Mulay, S., Desjardins, R., Day, R., Karaplis, A. C., Tremblay, M. L., and Canaff, L. (2006) *Mol. Endocrinol.* **20,** 1935–1947
16. Corradi, N., Borgonovo, B., Clementi, E., Bassetti, M., Racchetti, G., Consalez, G. G., Huttner, W. B., Meldolesi, J., and Rosa, P. (1996) *J. Biol. Chem.* **271,** 27116–27124
17. Inomoto, C., Umemura, S., Egashira, N., Minematsu, T., Takekoshi, S., Itoh, Y., Itoh, J., Taupenot, L., O'Connor, D. T., and Osamura, R. Y. (2007) *J. Histochem. Cytochem.* **55,** 487–493
18. Stettler, H., Beuret, N., Prescianotto-Baschong, C., Fayard, B., Taupenot, L., and Spiess, M. (2009) *Biochem. J.* **418,** 81–91
19. Beuret, N., Stettler, H., Renold, A., Rutishauser, J., and Spiess, M. (2004) *J. Biol. Chem.* **279,** 20242–20249
20. Montero-Hadjadje, M., Elias, S., Chevalier, L., Benard, M., Tanguy, Y., Turquier, V., Galas, L., Yon, L., Malagon, M. M., Driouich, A., Gasman, S., and Anouar, Y. (2009) *J. Biol. Chem.* **284,** 12420–12431
21. Fischer-Colbrie, R., Hagn, C., and Schober, M. (1987) *Ann. N.Y. Acad. Sci.* **493,** 120–134
22. Egger, M., Schgoer, W., Beer, A. G., Jeschke, J., Leierer, J., Theurl, M., Frauscher, S., Tepper, O. M., Niederwanger, A., Ritsch, A., Kearney, M., Wanschitz, J., Gurtner, G. C., Fischer-Colbrie, R., Weiss, G., Piza-Katzer, H., Losordo, D. W., Patsch, J. R., Schratzberger, P., and Kirchmair, R. (2007) *FASEB J.* **21,** 2906–2917
23. Courel, M., Vasquez, M. S., Hook, V. Y., Mahata, S. K., and Taupenot, L. (2008) *J. Biol. Chem.* **283,** 11807–11822
24. Campbell, R. E., Tour, O., Palmer, A. E., Steinbach, P. A., Baird, G. S., Zacharias, D. A., and Tsien, R. Y. (2002) *Proc. Natl. Acad. Sci. U.S.A.* **99,** 7877–7882
25. El Meskini, R., Jin, L., Marx, R., Bruzzaniti, A., Lee, J., Emeson, R., and Mains, R. (2001) *Endocrinology* **142,** 864–873
26. Fisher, R. J., and Burgoyne, R. D. (1999) *Pflugers Arch.* **437,** 754–762
27. Pance, A., Morgan, K., Guest, P. C., Bowers, K., Dean, G. E., Cutler, D. F., and Jackson, A. P. (1999) *J. Neurochem.* **73,** 21–30
28. Taupenot, L., Harper, K. L., Mahapatra, N. R., Parmer, R. J., Mahata, S. K., and O'Connor, D. T. (2002) *J. Cell Sci.* **115,** 4827–4841
29. Reynolds, A., Leake, D., Boese, Q., Scaringe, S., Marshall, W. S., and Khvorova, A. (2004) *Nat. Biotechnol.* **22,** 326–330
30. Miller, V. M., Xia, H., Marrs, G. L., Gouvion, C. M., Lee, G., Davidson, B. L., and Paulson, H. L. (2003) *Proc. Natl. Acad. Sci. U.S.A.* **100,** 7195–7200
31. Eskeland, N. L., Zhou, A., Dinh, T. Q., Wu, H., Parmer, R. J., Mains, R. E., and O'Connor, D. T. (1996) *J. Clin. Invest.* **98,** 148–156
32. Reaves, B. J., Bright, N. A., Mullock, B. M., and Luzio, J. P. (1996) *J. Cell Sci.* **109,** 749–762
33. McCaffery, J. M., and Farquhar, M. G. (1995) *Methods Enzymol.* **257,** 259–279
34. Axelrod, D. (2003) *Methods Enzymol.* **361,** 1–33
35. Steyer, J. A., and Almers, W. (1999) *Biophys. J.* **76,** 2262–2271
36. Taylor, C. V., Taupenot, L., Mahata, S. K., Mahata, M., Wu, H., Yasothornsrikul, S., Toneff, T., Caporale, C., Jiang, Q., Parmer, R. J., Hook, V. Y., and O'Connor, D. T. (2000) *J. Biol. Chem.* **275,** 22905–22915
37. Taupenot, L., Harper, K. L., and O'Connor, D. T. (2005) *J. Biol. Chem.* **280,** 3885–3897
38. Montesinos, M. S., Machado, J. D., Camacho, M., Diaz, J., Morales, Y. G., Alvarez de la Rosa, D., Carmona, E., Castañeyra, A., Viveros, O. H.,

O'Connor, D. T., Mahata, S. K., and Borges, R. (2008) *J. Neurosci.* **28,** 3350–3358
39. Pedrazzini, T., Pralong, F., and Grouzmann, E. (2003) *Cell. Mol. Life Sci.* **60,** 350–377
40. Lang, T., Wacker, I., Steyer, J., Kaether, C., Wunderlich, I., Soldati, T., Gerdes, H. H., and Almers, W. (1997) *Neuron* **18,** 857–863
41. Tsuboi, T., and Fukuda, M. (2007) *Genes Cells* **12,** 511–519
42. Brun, C., Philip-Couderc, P., Raggenbass, M., Roatti, A., and Baertschi, A. J. (2006) *FASEB J.* **20,** 732–734
43. Kaipio, K., Kallio, J., and Pesonen, U. (2005) *Biochem. Biophys. Res. Commun.* **337,** 633–640
44. Kaipio, K., and Pesonen, U. (2009) *Neurosci. Lett.* **450,** 181–185
45. Silva, A. P., Cavadas, C., Baisse-Agushi, B., Spertini, O., Brunner, H. R., and Grouzmann, E. (2003) *Regul. Pept.* **116,** 71–79
46. Pance, A., Livesey, F. J., and Jackson, A. P. (2006) *J. Neurochem.* **99,** 1435–1444
47. Malosio, M. L., Giordano, T., Laslop, A., and Meldolesi, J. (2004) *J. Cell Sci.* **117,** 743–749
48. Twiss, J. L., and Shooter, E. M. (1995) *J. Neurochem.* **64,** 550–557
49. Mu, F. T., Callaghan, J. M., Steele-Mortimer, O., Stenmark, H., Parton, R. G., Campbell, P. L., McCluskey, J., Yeo, J. P., Tock, E. P., and Toh, B. H. (1995) *J. Biol. Chem.* **270,** 13503–13511
50. Taupenot, L. (2007) *Curr. Protoc. Cell Biol.* **Suppl. 36,** 15.12.1–15.12.13
51. Oheim, M., Loerke, D., Stühmer, W., and Chow, R. H. (1998) *Eur. Biophys. J.* **27,** 83–98
52. Burke, N. V., Han, W., Li, D., Takimoto, K., Watkins, S. C., and Levitan, E. S. (1997) *Neuron* **19,** 1095–1102
53. Tooze, S. A., Flatmark, T., Tooze, J., and Huttner, W. B. (1991) *J. Cell Biol.* **115,** 1491–1503
54. Tooze, S. A. (1991) *FEBS Lett.* **285,** 220–224
55. Wu, M. M., Grabe, M., Adams, S., Tsien, R. Y., Moore, H. P., and Machen, T. E. (2001) *J. Biol. Chem.* **276,** 33027–33035
56. Han, W., Li, D., Stout, A. K., Takimoto, K., and Levitan, E. S. (1999) *J. Neurosci.* **19,** 900–905
57. Carnell, L., and Moore, H. P. (1994) *J. Cell Biol.* **127,** 693–705
58. Urbé, S., Page, L. J., and Tooze, S. A. (1998) *J. Cell Biol.* **143,** 1831–1844
59. Mosley, C. A., Taupenot, L., Biswas, N., Taulane, J. P., Olson, N. H., Vaingankar, S. M., Wen, G., Schork, N. J., Ziegler, M. G., Mahata, S. K., and O'Connor, D. T. (2007) *Biochemistry* **46,** 10999–11012
60. Videen, J. S., Mezger, M. S., Chang, Y. M., and O'Connor, D. T. (1992) *J. Biol. Chem.* **267,** 3066–3073
61. Mahapatra, N. R., Taupenot, L., Courel, M., Mahata, S. K., and O'Connor, D. T. (2008) *Biochemistry* **47,** 7167–7178
62. Day, R., and Gorr, S. U. (2003) *Trends Endocrinol. Metab.* **14,** 10–13
63. Tischler, A. S., and Greene, L. A. (1978) *Lab. Invest.* **39,** 77–89
64. D'Alessandro, R., Klajn, A., Stucchi, L., Podini, P., Malosio, M. L., and Meldolesi, J. (2008) *J. Neurochem.* **105,** 1369–1383
65. Allersma, M. W., Wang, L., Axelrod, D., and Holz, R. W. (2004) *Mol. Biol. Cell* **15,** 4658–4668
66. Xiong, J., Li, D., Zhu, D., and Qu, A. (2005) in *Proceedings of 27th Annual International Conference of the IEEE*, Engineering in Medicine and Biology Society, Shanghai, China, September 1–4, 2005, pp. 7529–7532, IEEE Publishing, Los Alamitos, CA
67. Park, J. J., and Loh, Y. P. (2008) *Mol. Endocrinol.* **22,** 2583–2595
68. Haigh, J. R., and Phillips, J. H. (1989) *Biochem. J.* **257,** 499–507
69. Mahapatra, N. R., Mahata, M., Hazra, P. P., McDonough, P. M., O'Connor, D. T., and Mahata, S. K. (2004) *J. Biol. Chem.* **279,** 51107–51121
70. Ashley, R. H., Brown, D. M., Apps, D. K., and Phillips, J. H. (1994) *Eur. Biophys. J.* **23,** 263–275
71. Schoonderwoert, V. T., Holthuis, J. C., Tanaka, S., Tooze, S. A., and Martens, G. J. (2000) *Eur. J. Biochem.* **267,** 5646–5654
72. Tanaka, S., Yora, T., Nakayama, K., Inoue, K., and Kurosumi, K. (1997) *J. Histochem. Cytochem.* **45,** 425–436
73. Voorberg, J., Fontijn, R., Calafat, J., Janssen, H., van Mourik, J. A., and Pannekoek, H. (1993) *EMBO J.* **12,** 749–758
74. Yoo, S. H. (1993) *Biochemistry* **32,** 8213–8219
75. Yoo, S. H. (1995) *Biochemistry* **34,** 8680–8686
76. Han, L., Suda, M., Tsuzuki, K., Wang, R., Ohe, Y., Hirai, H., Watanabe, T., Takeuchi, T., and Hosaka, M. (2008) *Mol. Endocrinol.* **22,** 1935–1949
77. Hosaka, M., Suda, M., Sakai, Y., Izumi, T., Watanabe, T., and Takeuchi, T. (2004) *J. Biol. Chem.* **279,** 3627–3634
78. Hosaka, M., Watanabe, T., Sakai, Y., Uchiyama, Y., and Takeuchi, T. (2002) *Mol. Biol. Cell* **13,** 3388–3399
79. Prasad, P., Yanagihara, A. A., Small-Howard, A. L., Turner, H., and Stokes, A. J. (2008) *J. Immunol.* **181,** 5024–5034
80. Hotta, K., Hosaka, M., Tanabe, A., and Takeuchi, T. (2009) *J. Endocrinol.* **202,** 111–121
81. Grundschober, C., Malosio, M. L., Astolfi, L., Giordano, T., Nef, P., and Meldolesi, J. (2002) *J. Biol. Chem.* **277,** 36715–36724
82. Kim, T., and Loh, Y. P. (2006) *Mol. Biol. Cell* **17,** 789–798
83. Kim, T., Tao-Cheng, J. H., Eiden, L. E., and Loh, Y. P. (2002) *Ann. N.Y. Acad. Sci.* **971,** 323–331
84. Yoo, S. H., You, S. H., Kang, M. K., Huh, Y. H., Lee, C. S., and Shim, C. S. (2002) *J. Biol. Chem.* **277,** 16011–16021
85. Heidrich, F. M., Zhang, K., Estrada, M., Huang, Y., Giordano, F. J., and Ehrlich, B. E. (2008) *Circ. Res.* **102,** 1230–1238
86. Yoo, S. H., Chu, S. Y., Kim, K. D., and Huh, Y. H. (2007) *Biochemistry* **46,** 14663–14671
87. Yajima, A., Narita, N., and Narita, M. (2008) *J. Pept. Sci.* **14,** 773–776